Manipulation of type-I and type-II Dirac points in $PdTe_2$ superconductor by external pressure

R. C. Xiao,[1,2] P. L. Gong,[3] Q. S. Wu,[4] W. J. Lu,[1,*] M. J. Wei,[1,2] J. Y. Li,[1,2] H. Y. Lv,[1] X. Luo,[1] P. Tong,[1] X. B. Zhu,[1] and Y. P. Sun[1,5,6,†]

[1]*Key Laboratory of Materials Physics, Institute of Solid State Physics, Chinese Academy of Sciences, Hefei 230031, China*

[2]*University of Science and Technology of China, Hefei 230026, China*

[3]*Department of Physics, Southern University of Science and Technology, Shenzhen 518055, China*

[4]*Theoretical Physics and Station Q Zurich, ETH Zurich, Zurich 8093, Switzerland*

[5]*High Magnetic Field Laboratory, Chinese Academy of Sciences, Hefei 230031, China*

[6]*Collaborative Innovation Center of Microstructures, Nanjing University, Nanjing 210093, China*

(Received 8 May 2017; published 1 August 2017)

A pair of type-II Dirac cones in $PdTe_2$ was recently predicted by theories and confirmed in experiments, making $PdTe_2$ the first material that processes both superconductivity and type-II Dirac fermions. In this paper, we study the evolution of Dirac cones in $PdTe_2$ under hydrostatic pressure by first-principles calculations. Our results show that the pair of type-II Dirac points disappears at 6.1 GPa. Interestingly, a new pair of type-I Dirac points from the same two bands emerges at 4.7 GPa. Due to the distinctive band structures compared with those of $PtSe_2$ and $PtTe_2$, the two types of Dirac points can coexist in $PdTe_2$ under proper pressure (4.7–6.1 GPa). The emergence of type-I Dirac cones and the disappearance of type-II Dirac ones are attributed to an increase/decrease of the energy of the states at the Γ and A points, which have antibonding/bonding characters of the interlayer Te-Te atoms. On the other hand, we find that the superconductivity of $PdTe_2$ slightly decreases with pressure. The pressure-induced types of Dirac cones combined with superconductivity may open a promising way to investigate the complex interactions between Dirac fermions and superconducting quasiparticles.

DOI: 10.1103/PhysRevB.96.075101

I. INTRODUCTION

Topological (Dirac/Weyl) semimetals [1,2] are new topological states of three-dimensional (3D) quantum matter, different from topological insulators. In Dirac/Weyl semimetals, the linear band crossings are fourfold/twofold degenerated points, whose low-energy excitations are massless Dirac/Weyl fermions corresponding to their counterparts in high-energy physics. By breaking inversion symmetry or time-reversal symmetry, one Dirac fermion will transform into two Weyl ones with opposite chiralities in the Brillouin zone (BZ). In recent years, the discoveries of Dirac semimetals (such as Na_3Bi [3,4] and Cd_3As_2 [5–7]) and Weyl semimetals (such as $Y_2Ir_2O_7$ [8], $HgCr_2Se_4$ [9], and TaAs [10–12]) in theories and/or experiments made Dirac and Weyl fermions widely considered.

The Dirac/Weyl semimetals that directly correspond to their counterparts in high-energy physics are usually called type-I Dirac/Weyl semimetals. However, unlike high-energy physics, the restriction of Lorentz invariance is not necessary in condensed matter physics. Recently, a great deal of attention was paid to look for new topological quasiparticles beyond the direct counterparts in high-energy physics [13]. Soluyanov *et al.* [14] proposed a new type of Weyl fermion (type II) that contacts the bulk electron and hole pockets in condensed matter systems. Afterwards, many type-II Weyl semimetals were discovered, such as WTe_2 [14–17], $MoTe_2$ [18–20], $Mo_xW_{1-x}Te_2$ [21,22], Ta_3S_2 [23], $TaIrTe_4$ [24], and LaAlGe [25]. Type-II Weyl semimetals show exotic properties different from type-I ones, such as direction-dependent chiral anomaly [14,26,27], enhanced superconductivity [28,29], antichiral effect of the chiral Landau level [30], and novel quantum oscillations [31].

Researchers are also trying to find type-II Dirac fermions in condensed matter. Recently, Huang *et al.* [32] predicted that type-II Dirac fermions protected by C_3 rotational symmetry can exist in the $PtSe_2$ family of materials, and similar proposals were also put forward by Le *et al.* [33] and Chang *et al.* [34] in the KMgBi and VAl_3 family of materials, respectively. Following Huang's predictions, evidence of type-II Dirac cones in $PtTe_2$ [35,36], $PdTe_2$ [36–38], and $PtSe_2$ [36,39] was soon characterized in angle-resolved photoemission spectroscopy (ARPES) experiments by different groups. Similar to type-II Weyl cones, type-II Dirac cones are strongly tilted in some specific directions. Novel physical properties different from those in standard type-I Dirac semimetals are expected in type-II Dirac semimetals [32,34]. Interestingly, $PdTe_2$ is also a superconductor with a transition temperature (T_C) of about 1.7–2.0 K [37,40,41]. The coexistence of superconductivity and type-II Dirac points in $PdTe_2$ makes it significantly different from other members of the $PtSe_2$ family of materials, which could provide a possible platform to explore the interplay between superconducting quasiparticles and Dirac fermions [36–38].

Pressure can drive topological phase transitions in topological materials and can also assist in comprehending the nature of topological states at ambient pressure. In this paper, we focus on studying the evolution of Dirac points and superconductivity in $PdTe_2$ under hydrostatic pressure by first-principles calculations. Our results show that the pair of type-II Dirac points disappears at 6.1 GPa, while a new pair of type-I Dirac points emerges at 4.7 GPa. Under a pressure of 4.7–6.1 GPa, type-II and type-I Dirac cones coexist. The evolution of the two types of Dirac cones can be understood by bonding

*wjlu@issp.ac.cn
†ypsun@issp.ac.cn

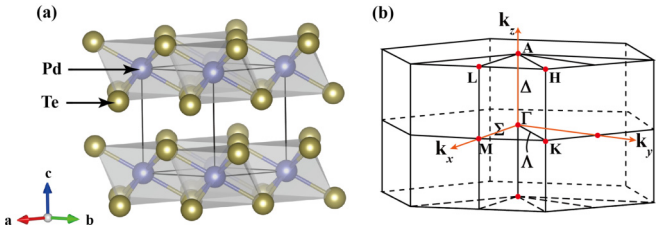

FIG. 1. (a) Crystal structure and (b) Brillouin zone of $PdTe_2$.

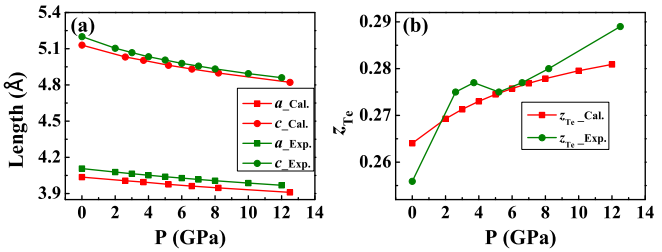

FIG. 2. (a) Lattice constants and (b) z_{Te} of $PdTe_2$ under pressure. Experimental data are from Ref. [46].

and antibonding characters near the Dirac cones. We also find that superconductivity slowly decreases with an increase of pressure, meaning that there are abundant topological transitions together with superconductivity in $PdTe_2$ under an external pressure.

II. METHOD

First-principles calculations based on density functional theory (DFT) were performed using the QUANTUM ESPRESSO package [42]. Ultrasoft pseudopotentials and generalized gradient approximation (GGA) according to the Perdew-Burke-Ernzerhof (PBE) functional were used. The energy cutoff of the plane wave (charge density) basis was set to 50 Ry (500 Ry). The BZ was sampled with a $12 \times 12 \times 8$ mesh of k points. The Methfessel-Paxton Fermi smearing method with a smearing parameter of $\sigma = 0.02$ Ry was used. The lattice constants and ions were optimized using the Broyden-Fletcher-Goldfarb-Shanno (BFGS) quasi-Newton algorithm. All of the band structure calculations were cross checked by the VASP codes [43,44], and the results were consistent with each other.

III. RESULTS AND DISCUSSION

$PdTe_2$ belongs to transition metal dichalcogenides (TMDCs), and has a layered structure with space group $P\bar{3}m1$ ($1T$-CdI_2 type structure) with one Pd atom and two Te atoms located at the (0,0,0) and $(1/3,2/3,\pm z_{Te})$ sites, respectively [Fig. 1(a)]. One Pd atom and the nearest six Te atoms compose an octahedron. The lattice constant ratio c/a ($\approx$1.27) is the smallest among the isostructural TMDCs [45], leading to the octahedra being largely distorted. The special k points and the paths of BZ are shown in Fig. 1(b), and the corresponding symmetries are summarized in Table S1 in the Supplemental Material [47]. The calculated lattice constants a and c at ambient pressure are slightly overestimated by about 1.76% and 1.36%, respectively, due to the underestimation of the bond strength in GGA. No structural phase transition was found up to 27 GPa in the experiment [46]. The optimized lattice constants under pressure are shown in Fig. 2.

The band structures along the Γ-A direction at ambient pressure without/with spin-orbit coupling (SOC) effects are shown in Fig. 3. Without SOC, the E band (denoted by the green color) and the A_1 band (denoted by the red color), which belong to two different irreducible representations (IRs), cross each other near the A point. The E band is mainly composed of Te-$p_x + p_y$ orbitals, while the A_1 band is mainly composed of Te-p_z orbitals (see Fig. S1 in the Supplemental Material [47]), leading to the A_1 band (red) being more dispersive than the E band (green). When SOC is included, the band structures change dramatically, as shown in Fig. 3(b). All the A_1 bands transform into two-dimensional (2D) IR Δ_4 bands, and all the E bands split into Δ_4 (2D IR) and Δ_{5+6} bands [the Δ_5 (1D IR) and Δ_6 (1D IR) bands are degenerated along the Γ-A direction]. The band crossing near the A point is also inevitable with SOC, since the Δ_4 (red) and Δ_{5+6} (green) bands belong to different 2D IRs. The strongly dispersive band Δ_4 crosses the less dispersive band Δ_{5+6}, resulting in a titled Dirac cone along k_z, which is the type-II Dirac cone previously proposed by theories and verified in ARPES experiments [36–38]. The type-II Dirac cone protected by C_3 rotational symmetry is tilted along the Γ-A direction but untilted on the k_x-k_y plane. According to the crystal symmetry, there is another type-II Dirac point located at the opposite position of the BZ, thus there is a pair of type-II Dirac cones. The location of the pair of type-II Dirac points in $PdTe_2$ is closer to the Fermi energy (E_F) than those of $PtSe_2$ and $PdTe_2$ [32].

Because the Δ_4 band (red) and the upper Δ_4 band (black) belong to the same IR, as a result, a band inversion at the Γ point instead of a band crossing at the Γ-A direction occurs [Fig. 3(b)]. A topological surface state located at $\bar{\Gamma}$ deeply below E_F at -1.75 eV was observed in the experiments, which was considered to be due to band inversion between the two lowest Δ_4 bands in Fig. 3(b) [36,38,40].

The A_4^+ state moves upward while the A_{5+6}^- state moves downward relative to E_F with pressure [Figs. 4(a)–4(e)], thus this pair of type-II Dirac cones gradually disappears near the

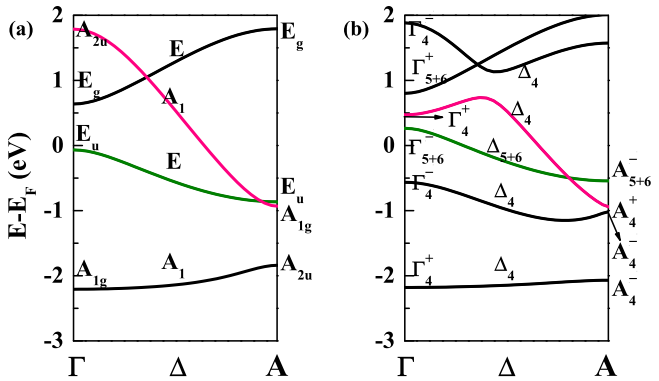

FIG. 3. Band structures of $PdTe_2$ (a) without and (b) with SOC along the Γ-A direction at ambient pressure. The irreducible representations are indicated. The band symmetries are also denoted near each band, and the IRs are introduced in Tables S2– S5 in the Supplemental Material [47].

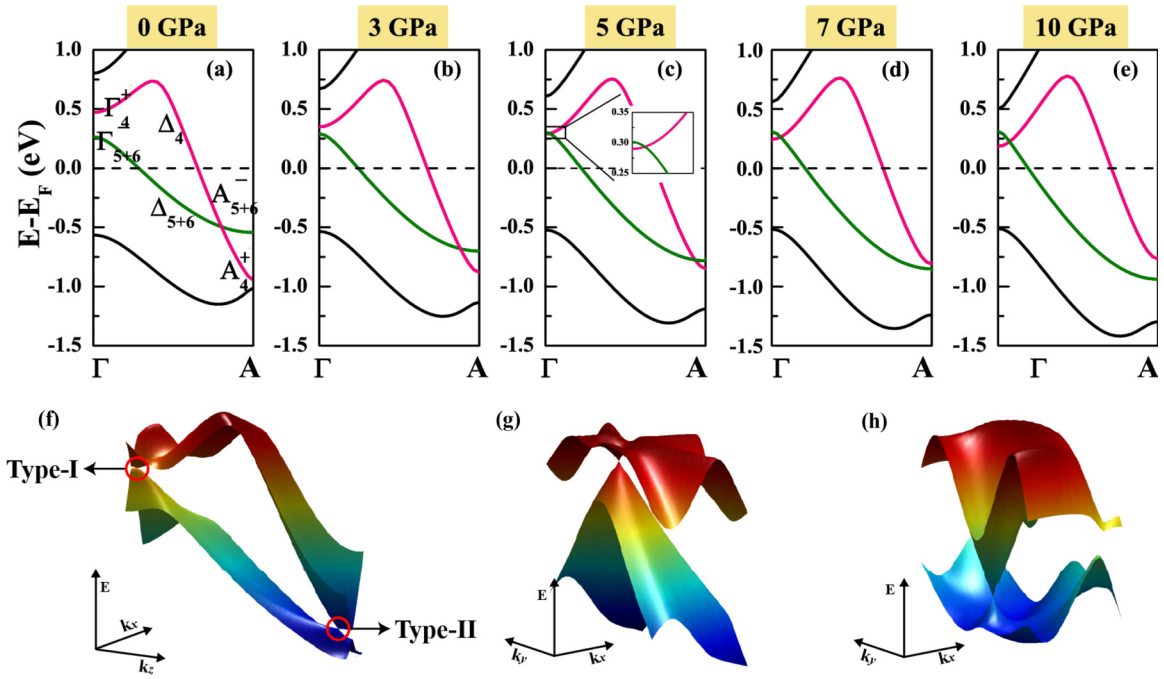

FIG. 4. (a)–(e) Evolution of the Dirac points of $PdTe_2$ from 0 to 10 GPa. 3D band structures at 5 GPa on the (f) k_x-k_z plane, (g) $k_z = 0.012\ 2\pi/c$ plane around the type-I Dirac cone, and (h) $k_z = 0.468\ 2\pi/c$ plane around the type-II Dirac cone. The band structures at 5 GPa along the in-plane and out-of-plane directions are shown in Fig. S3 in the Supplemental Material [47].

A point. The Γ_4^+ state moves downward while the Γ_{5+6}^- state moves upward with pressure, so a new pair of untitled Dirac points, i.e., type-I Dirac points, from the same two bands emerges near the Γ point. The energy evolution of the Γ_4^+, Γ_{5+6}^-, A_4^+, and A_{5+6}^- states under pressure is summarized in Fig. 5(a), from which we can see that a pair of type-I Dirac cones emerges at 4.7 GPa, and the pair of type-II Dirac cones disappears at 6.1 GPa. Under a pressure of 4.7–6.1 GPa, the two kinds of Dirac points coexist [for instance, the 3D band structures at 5 GPa in Figs. 4(f)–4(h)]. When pressure is further increased, only the pair of type-I Dirac cones remains. The energy and positions of the two kinds of Dirac points are shown in Figs. 5(b) and 5(c). The type-II and type-I Dirac points are located below and above E_F, respectively, and both move downward with pressure. Under higher pressure (about 30 GPa) the pair of type-I Dirac points will move to E_F. In the coexistence range, the type-II and type-I Dirac points are well separated in the BZ, which can be easily detected in experiments.

To reveal why type-II Dirac points disappear and type-I Dirac points emerge, the charge density of the Γ_4^+, Γ_{5+6}^-, A_4^+, and A_{5+6}^- states in real space was calculated and is shown in Fig. 6. The interlayer Te-Te atoms show a bonding character

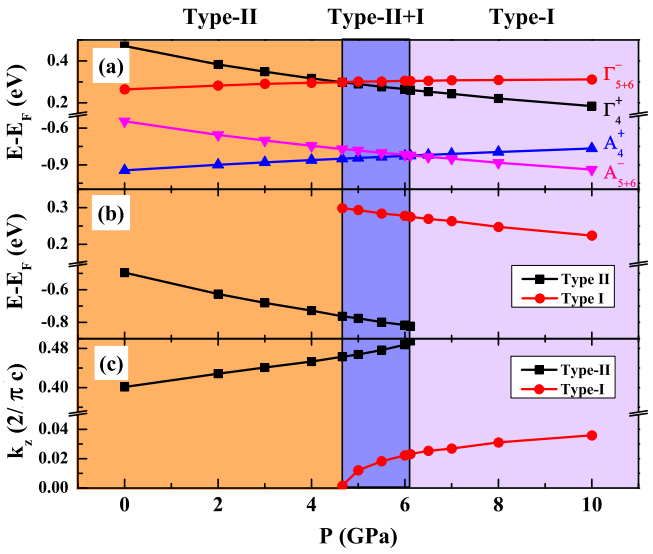

FIG. 5. (a) Energy evolution of the Γ_4^+, Γ_{5+6}^-, A_4^+, and A_{5+6}^- states of $PdTe_2$ under pressure. (b) Energy and (c) positive positions of type-II and type-I Dirac points under pressure. The regions decorated by colors stand for the existing ranges of the Dirac cones.

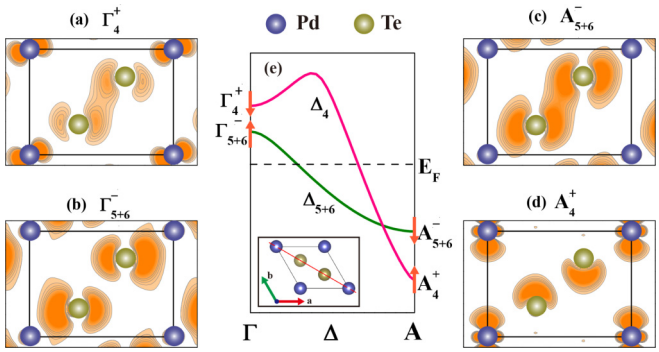

FIG. 6. Charge density of the (a) Γ_4^+, (b) Γ_{5+6}, (c) A_{5+6}^-, and (d) A_4^+ states of $PdTe_2$ in the (110) plane at ambient pressure. The arrows in (e) denote the moving directions under pressure, and the inset illustrates the (110) plane.

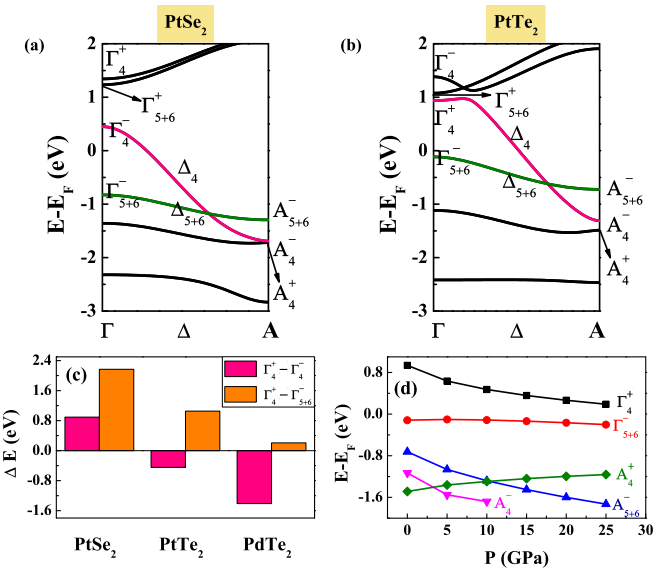

FIG. 7. Band structures of (a) $PtSe_2$ and (b) $PtTe_2$ along the Γ-A direction. (c) Inversion energy of Γ_4^+ and Γ_4^- states and energy difference of Γ_4^+ and Γ_{5+6}^- states for three materials at ambient pressure. (d) Energy evolution of Γ_4^+, Γ_{5+6}^-, A_4^+, and A_{5+6}^- states of $PtTe_2$ under pressure. The A_4^+ and A_4^- states are inverse with pressure (see Fig. S5).

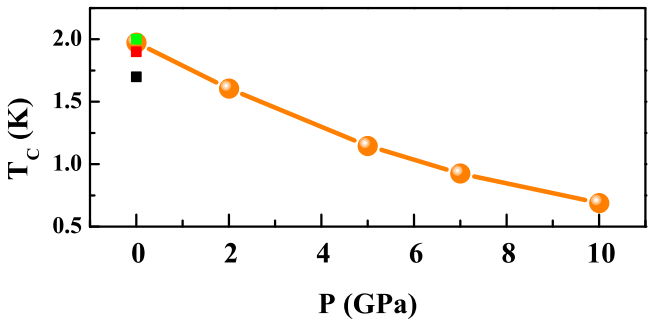

FIG. 8. Calculated T_C of $PdTe_2$ under pressure (orange balls). The squares at ambient pressure indicate the experimentally detected values. The black square is from Refs. [40,51], the red one is from Ref. [37], and the green one is from Ref. [41].

in the Γ_4^+ [Fig. 6(a)] and A_{5+6}^- [Fig. 6(c)] states, while the interlayer Te-Te atoms show an antibonding character in the Γ_{5+6}^- [Fig. 6(b)] and A_4^+ [Fig. 6(d)] states. Since the interlayers bind to each other via a weak van der Waals interaction, and the Pd atom orbitals are localized and the Te atom orbitals are extended in the Γ_4^+ and A_4^+ states, the Te atom orbitals are more easily affected by pressure. Pressure decreases the atom distance and enhances the atom interaction, leading to the energy of the bonding states moving downward, and the energy of the antibonding states moving upward relative to E_F. The opposite bonding character of the Γ_4^+ and Γ_{5+6}^- states makes their energy move in opposite directions with pressure, and so do the A_4^+ and A_{5+6}^- states. The similar bonding and antibonding characters of the states make the topological phase transitions or metal-insulator transitions in Bi_2Se_3 [48] and phosphorene [49,50] under pressure. Just as the statement in Ref. [36], the formation of type-II Dirac cones is very general: It is due merely to the different dispersions of two IR bands. Pressure can manipulate the band inversion and band dispersion, so more type-II Dirac and type-I Dirac materials are expected to be found in TMDCs under pressure.

Due to the same crystal structure, $PtSe_2$ and $PdTe_2$ show band structures similar to $PdTe_2$ [see Figs. 7(a) and 7(b)]. However, differences also exist. The Γ_4^+ and Γ_4^- states are inverse in $PtTe_2$ [Fig. 7(b)] and $PdTe_2$ [Fig. 3(b)], but they are not inverse in $PtSe_2$ [Fig. 7(a)]. The inversion energy of the Γ_4^+ and Γ_4^- states (1.41 eV) is the largest, and the energy difference of the Γ_4^+ and Γ_{5+6}^- states (0.21 eV) is the smallest in $PdTe_2$ [see Fig. 7(c)]. Due to distinctive band structures, two kinds of Dirac points are easier to coexist in $PdTe_2$ compared with the cases of $PtSe_2$ and $PtTe_2$. Taking $PtTe_2$ as an example, the evolution of band structures under an external pressure in $PtTe_2$ (see Fig. S5 in the Supplemental Material [47]) is similar to that of $PdTe_2$. The A_4^+/A_{5+6}^- state of $PtTe_2$ moves upward/downward with pressure, and the pair of type-II Dirac points gradually disappears at about 10 GPa [see Fig. 7(d)]. Meanwhile the $\Gamma_4^+/\Gamma_{5+6}^-$ state moves downward/upward with pressure, and a new pair of type-I Dirac points will emerge at a higher pressure. However, type-II and type-I Dirac points do not coexist in $PtTe_2$ under pressure. A similar evaluation of Dirac points in $PtSe_2$ is summarized in the Supplemental Material [47].

We also evaluated the phonon and electron-phonon coupling of $PdTe_2$ under pressure. The phonon branches become more dispersive and shift to a higher frequency with pressure. The calculated T_C decreases slowly with a nearly linear rate of 0.13 K/GPa from 1.97 K at ambient pressure to 0.69 K at 10 GPa (see Fig. 8). The decrease in the electronic density of states at E_F [$N(E_F)$] and the blueshift of the phonon density of states [$F(\omega)$] contribute to the decrease of T_C. Although T_C decreases monotonously with pressure, it is still in an experimentally detectable range. Especially, T_C is above 1.0 K in the coexistence range of the two types of Dirac cones. Detailed discussions may be found in the Supplemental Material [47].

The intrinsic topology property can drive conventional superconductivity into nontrivial p-wave-like unconventional topological superconductivity via a conventional phonon mediated mechanism [52,53], such as doped Bi_2Se_3 [53–57] and pressed Cd_3As_2 [58,59]. Thus the issue of whether $PdTe_2$ is a topological superconductor needs to be investigated further. The electron and hole pockets near the type-II Dirac points provide a larger density of states than those of the type-I Dirac points due to the tilted cones. As the type-II Weyl points [28,29], type-II Dirac points are favorable for both superconducting and topological superconducting carrier ratios [37]. As for the coexistence of type-I and type-II Dirac points in $PdTe_2$, more superconducting carrier ratios could be expected, and more interesting superconductivity properties should appear, which deserves to be investigated further.

In addition, because the lattice constants under pressure optimized by GGA show about a 2% systematic overestimation with the experimental data [46], we calculated the band structures using the experimental data to estimate the overestimation (see Fig. S11 in the Supplemental Material [47]). The pairs of type-II and type-I Dirac cones can still coexist

under proper pressure when the experimental lattice constants are adopted, and the transition pressure of the Dirac points may be smaller than that using the optimized structure data.

IV. CONCLUSION

Type-I and type-II Dirac points in $PdTe_2$ can be tuned by applying external pressure. The pair of type-II Dirac points disappears with pressure at 6.1 GPa, while a new pair of type-I Dirac points stemming from the same bands emerges at 4.7 GPa. The two types of Dirac points can coexist under proper pressure (4.7–6.1 GPa). The increase of the A_4^+ state energy and the decrease of the A_{5+6}^- state energy make the pair of type-II Dirac points gradually disappear. The increase of the Γ_{5+6}^- state energy and the decrease of the Γ_4^+ state energy make the type-I Dirac points emerge. The decrease/increase of the (Γ_4^+ and A_{5+6}^-)/(Γ_{5+6}^- and A_4^+) states' energies is attributed to the bonding/antibonding character of the interlayer Te-Te atoms. Due to the distinctive band structures of $PdTe_2$, the type-II and type-I Dirac points from the same two bands can coexist in $PdTe_2$ under appropriate pressures. Superconductivity weakens monotonously with pressure with an average rate of 0.13 K/GPa due to a decrease of $N(E_F)$ and the blueshift of $F(\omega)$, but it is still within an experimentally detectable range. Given the abundant topological transitions and superconductivity under pressure, $PdTe_2$ under pressure may be an interesting topological Dirac material. Further experimental verification and theoretical studies need to be addressed.

ACKNOWLEDGMENTS

This work was supported by the National Key Research and Development Program of China under Contract No. 2016YFA0300404, the National Nature Science Foundation of China under Contracts No. 11674326, No. 11404340, No. 11404024, and No. U1232139, Key Research Program of Frontier Sciences of CAS (QYZDB-SSW-SLH015), and Hefei Science Center of CAS (2016HSC-IU011). The calculations were partially performed at the Center for Computational Science, CASHIPS. Q.S.W. was supported by Microsoft Research, and the Swiss National Science Foundation through the National Competence Centers in Research MARVEL and QSIT. We also acknowledge Dr. Chi-Ho Cheung at National Taiwan University for useful discussions.

[1] H. Weng, X. Dai, and Z. Fang, J. Phys.: Condens. Matter. **28**, 303001 (2016).
[2] A. Bansil, H. Lin, and T. Das, Rev. Mod. Phys. **88**, 021004 (2016).
[3] Z. Wang, Y. Sun, X.-Q. Chen, C. Franchini, G. Xu, H. Weng, X. Dai, and Z. Fang, Phys. Rev. B **85**, 195320 (2012).
[4] Z. K. Liu, B. Zhou, Y. Zhang, Z. J. Wang, H. M. Weng, D. Prabhakaran, S.-K. Mo, Z. X. Shen, Z. Fang, X. Dai *et al.*, Science **343**, 864 (2014).
[5] Z. Wang, H. Weng, Q. Wu, X. Dai, and Z. Fang, Phys. Rev. B **88**, 125427 (2013).
[6] M. Neupane, S.-Y. Xu, R. Sankar, N. Alidoust, G. Bian, C. Liu, I. Belopolski, T.-R. Chang, H.-T. Jeng, H. Lin *et al.*, Nat. Commun. **5**, 3786 (2014).
[7] S. Borisenko, Q. Gibson, D. Evtushinsky, V. Zabolotnyy, B. Buchner, and R. J. Cava, Phys. Rev. Lett. **113**, 027603 (2014).
[8] X. Wan, A. M. Turner, A. Vishwanath, and S. Y. Savrasov, Phys. Rev. B **83**, 205101 (2011).
[9] G. Xu, H. Weng, Z. Wang, X. Dai, and Z. Fang, Phys. Rev. Lett. **107**, 186806 (2011).
[10] H. Weng, C. Fang, Z. Fang, B. A. Bernevig, and X. Dai, Phys. Rev. X **5**, 011029 (2015).
[11] B. Q. Lv, H. M. Weng, B. B. Fu, X. P. Wang, H. Miao, J. Ma, P. Richard, X. C. Huang, L. X. Zhao, G. F. Chen *et al.*, Phys. Rev. X **5**, 031013 (2015).
[12] S.-Y. Xu, I. Belopolski, N. Alidoust, M. Neupane, G. Bian, C. Zhang, R. Sankar, G. Chang, Z. Yuan, C.-C. Lee *et al.*, Science **349**, 613 (2015).
[13] Y. Xu, F. Zhang, and C. Zhang, Phys. Rev. Lett. **115**, 265304 (2015).
[14] A. A. Soluyanov, D. Gresch, Z. Wang, Q. Wu, M. Troyer, X. Dai, and B. A. Bernevig, Nature (London) **527**, 495 (2015).
[15] Y. Wu, D. Mou, N. H. Jo, K. Sun, L. Huang, S. L. Bud'ko, P. C. Canfield, and A. Kaminski, Phys. Rev. B **94**, 121113 (2016).
[16] C. Wang, Y. Zhang, J. Huang, S. Nie, G. Liu, A. Liang, Y. Zhang, B. Shen, J. Liu, C. Hu *et al.*, Phys. Rev. B **94**, 241119 (2016).
[17] F. Y. Bruno, A. Tamai, Q. S. Wu, I. Cucchi, C. Barreteau, A. de la Torre, S. McKeown Walker, S. Riccó, Z. Wang, T. K. Kim *et al.*, Phys. Rev. B **94**, 121112 (2016).
[18] Y. Sun, S. C. Wu, M. N. Ali, C. Felser, and B. Yan, Phys. Rev. B **92**, 161107(R) (2015).
[19] Z. Wang, D. Gresch, A. A. Soluyanov, W. Xie, S. Kushwaha, X. Dai, M. Troyer, R. J. Cava, and B. A. Bernevig, Phys. Rev. Lett. **117**, 056805 (2016).
[20] A. Tamai, Q. S. Wu, I. Cucchi, F. Y. Bruno, Riccó S, T. K. Kim, M. Hoesch, C. Barreteau, E. Giannini, C. Besnard *et al.*, Phys. Rev. X **6**, 031021 (2016).
[21] I. Belopolski, S. Y. Xu, Y. Ishida, X. Pan, P. Yu, D. S. Sanchez, H. Zheng, M. Neupane, N. Alidoust, G. Chang *et al.*, Phys. Rev. B **94**, 085127 (2016).
[22] T. R. Chang, S. Y. Xu, G. Chang, C. C. Lee, S. M. Huang, B. Wang, G. Bian, H. Zheng, D. S. Sanchez, I. Belopolski *et al.*, Nat. Commun. **7**, 10639 (2016).
[23] G. Chang, S.-Y. Xu, D. S. Sanchez, S.-M. Huang, C.-C. Lee, T.-R. Chang, G. Bian, H. Zheng, I. Belopolski, N. Alidoust *et al.*, Sci. Adv. **2**, e1600295 (2016).
[24] K. Koepernik, D. Kasinathan, D. V. Efremov, S. Khim, S. Borisenko, B. Büchner, and J. van den Brink, Phys. Rev. B **93**, 201101 (2016).
[25] S.-Y. Xu, N. Alidoust, G. Chang, H. Lu, B. Singh, I. Belopolski, D. S. Sanchez, X. Zhang, G. Bian, H. Zheng *et al.*, arXiv:1603.07318.
[26] Y.-Y. Lv, X. Li, B.-B. Zhang, W. Y. Deng, S.-H. Yao, Y. B. Chen, J. Zhou, S.-T. Zhang, M.-H. Lu, L. Zhang *et al.*, Phys. Rev. Lett. **118**, 096603 (2017).

[27] M. Udagawa and E. J. Bergholtz, Phys. Rev. Lett. **117**, 086401 (2016).
[28] M. Alidoust, K. Halterman, and A. A. Zyuzin, Phys. Rev. B **95**, 155124 (2017).
[29] D. Li, B. Rosenstein, B. Y. Shapiro, and I. Shapiro, Phys. Rev. B **95**, 094513 (2017).
[30] Z.-M. Yu, Y. Yao, and S. A. Yang, Phys. Rev. Lett. **117**, 077202 (2016).
[31] T. E. O'Brien, M. Diez, and C. W. J. Beenakker, Phys. Rev. Lett. **116**, 236401 (2016).
[32] H. Huang, S. Zhou, and W. Duan, Phys. Rev. B **94**, 121117(R) (2016).
[33] C. Le, S. Qin, X. Wu, X. Dai, P. Fu, and J. Hu, arXiv:1606.05042.
[34] T.-R. Chang, S.-Y. Xu, D. S. Sanchez, W.-F. Tsai, S.-M. Huang, G. Chang, C.-H. Hsu, G. Bian, I. Belopolski, Z.-M. Yu *et al.*, Phys. Rev. Lett. **119**, 026404 (2017).
[35] M. Yan, H. Huang, K. Zhang, E. Wang, W. Yao, K. Deng, G. Wan, H. Zhang, M. Arita, H. Yang *et al.*, arXiv:1607.03643.
[36] M. S. Bahramy, O. J. Clark, B.-J. Yang, J. Feng, L. Bawden, J. M. Riley, I. Marković, F. Mazzola, V. Sunko, S. P. Cooil *et al.*, arXiv:1702.08177.
[37] F. Fei, X. Bo, R. Wang, B. Wu, J. Jiang, D. Fu, M. Gao, H. Zheng, Y. Chen, X. Wang *et al.*, Phys. Rev. B **96**, 041201 (2017).
[38] H.-J. Noh, J. Jeong, E.-J. Cho, K. Kim, B. I. Min, and B.-G. Park, Phys. Rev. Lett. **119**, 016401 (2017).
[39] K. Zhang, M. Yan, H. Zhang, H. Huang, M. Arita, Z. Sun, W. Duan, Y. Wu, and S. Zhou, arXiv:1703.04242.
[40] Y. Liu, J. Z. Zhao, L. Yu, C. T. Lin, A. J. Liang, C. Hu, Y. Ding, Y. Xu, S. L. He, L. Zhao *et al.*, Chin. Phys. Lett. **32**, 067303 (2015).
[41] Y. Wang, J. Zhang, W. Zhu, Y. Zou, C. Xi, L. Ma, T. Han, J. Yang, J. Wang, J. Xu *et al.*, Sci. Rep. **6**, 31554 (2016).
[42] P. Giannozzi, S. Baroni, N. Bonini, M. Calandra, R. Car, C. Cavazzoni, D. Ceresoli, G. L. Chiarotti, M. Cococcioni, I. Dabo *et al.*, J. Phys.: Condens. Matter **21**, 395502 (2009).
[43] G. Kresse and J. Furthmuller, Phys. Rev. B **54**, 11169 (1996).
[44] G. Kresse and D. Joubert, Phys. Rev. B **59**, 1758 (1999).
[45] J. A. Wilson and A. D. Yoffe, Adv. Phys. **18**, 193 (1969).
[46] C. Soulard, P. E. Petit, P. Deniard, M. Evain, S. Jobic, M. H. Whangbo, and A.-C. Dhaussy, J. Solid State Chem. **178**, 2008 (2005).
[47] See Supplemental Material at http://link.aps.org/supplemental/10.1103/PhysRevB.96.075101 for detailed information on the character tables for $\bar{3}m$ and $3m$, fat bands of $PdTe_2$, evolution of Dirac points of $PtTe_2$ and $PtSe_2$ under pressure, and results and discussions of superconductivity of $PdTe_2$ under pressure, which includes Refs. [60–69].
[48] J. Liu, Y. Xu, J. Wu, B.-L. Gu, S. B. Zhang, and W. Duan, Acta Crystallogr. C **70**, 118 (2014).
[49] A. Manjanath, A. Samanta, T. Pandey, and A. K. Singh, Nanotechnology **26**, 075701 (2015).
[50] C. Wang, Q. Xia, Y. Nie, and G. Guo, J. Appl. Phys. **117**, 124302 (2015).
[51] G. Ryu, J. Supercond. Novel Magn. **28**, 3275 (2015).
[52] G. Y. Cho, J. H. Bardarson, Y.-M. Lu, and J. E. Moore, Phys. Rev. B **86**, 214514 (2012).
[53] X. Wan and S. Y. Savrasov, Nat. Commun. **5**, 4144 (2014).
[54] Y. S. Hor, A. J. Williams, J. G. Checkelsky, P. Roushan, J. Seo, Q. Xu, H. W. Zandbergen, A. Yazdani, N. P. Ong, and R. J. Cava, Phys. Rev. Lett. **104**, 057001 (2010).
[55] T. V. Bay, T. Naka, Y. K. Huang, H. Luigjes, M. S. Golden, and A. de Visser, Phys. Rev. Lett. **108**, 057001 (2012).
[56] M.-X. Wang, C. Liu, J.-P. Xu, F. Yang, L. Miao, M.-Y. Yao, C. L. Gao, C. Shen, X. Ma, X. Chen *et al.*, Science **336**, 52 (2012).
[57] L. Fu, Phys. Rev. B **90**, 100509 (2014).
[58] H. Wang, H. Wang, H. Liu, H. Lu, W. Yang, S. Jia, X.-J. Liu, X. C. Xie, J. Wei, and J. Wang, Nat. Mater. **15**, 38 (2016).
[59] L. Aggarwal, A. Gaurav, G. S. Thakur, Z. Haque, A. K. Ganguli, and G. Sheet, Nat. Mater. **15**, 32 (2016).
[60] G. F. Koster, Solid State Phys. **5**, 173 (1957).
[61] S. Baroni, S. de Gironcoli, A. Dal Corso, and P. Giannozzi, Rev. Mod. Phys. **73**, 515 (2001).
[62] T. R. Finlayson, W. Reichardt, and H. G. Smith, Phys. Rev. B **33**, 2473 (1986).
[63] P. B. Allen and R. C. Dynes, Phys. Rev. B **12**, 905 (1975).
[64] R. C. Dynes, Solid State Commun. **10**, 615 (1972).
[65] M. Calandra and F. Mauri, Phys. Rev. Lett. **106**, 196406 (2011).
[66] E. S. Penev, A. Kutana, and B. I. Yakobson, Nano Lett. **16**, 2522 (2016).
[67] J. Kortus, I. I. Mazin, K. D. Belashchenko, V. P. Antropov, and L. L. Boyer, Phys. Rev. Lett. **86**, 4656 (2001).
[68] Y. Liu, J.-Z. Zhao, L. Yu, C.-T. Lin, C. Hu, D.-F. Liu, Y.-Y. Peng, Z.-J. Xie, J.-F. He, C.-Y. Chen *et al.*, Chin. Phys. B **24**, 067401 (2015).
[69] H. W. Myron, Solid State Commun. **15**, 395 (1974).